

We are IntechOpen, the world's leading publisher of Open Access books Built by scientists, for scientists

6,900

Open access books available

186,000

International authors and editors

200M

Downloads

Our authors are among the

154

Countries delivered to

TOP 1%

most cited scientists

12.2%

Contributors from top 500 universities



WEB OF SCIENCE™

Selection of our books indexed in the Book Citation Index
in Web of Science™ Core Collection (BKCI)

Interested in publishing with us?
Contact book.department@intechopen.com

Numbers displayed above are based on latest data collected.
For more information visit www.intechopen.com



Constant Dew Point Corrosion Tests for Metals

Zhenhua Dan, Izumi Muto and Nobuyoshi Hara

Additional information is available at the end of the chapter

<http://dx.doi.org/10.5772/57291>

1. Introduction

Aluminium alloys are widely used in the automobile industry, in construction and in other fields where energy consumption and environmental safety are a high priority due to their high strength-to-weight ratio, their infinite recycling properties and high corrosion resistance [1-3]. Besides the prohibitively high costs of maintaining degraded aluminium products degradation in the form of localized attacks has resulted in fatalities, particularly in Cl-containing environments. The atmospheric corrosion of aluminium alloys is therefore a research field which has been extensively investigated by many researchers and groups mostly using field exposure tests [4-8]. The complex combination of environmental factors in the outdoor atmosphere, such as the amounts of airborne salt and contamination species, as well as the ever-changing weather conditions, makes it difficult to clarify the corrosion process. Conventional laboratory scale tests have been employed to evaluate the atmospheric corrosion resistance of materials. Among them, the salt spray test (ASTM B117) is widely used as an acceleration test [9-11]. Cyclic corrosion tests, such as ASTM G85-A5 and SAE J2334, and constant relative humidity tests have also been used to simulate actual atmospheric corrosion at a laboratory level [12-14]. However, in terms of corrosion morphology, these tests do not always provide good reproducibility of practical atmospheric corrosion behaviour. By measuring fluctuations in the night and day temperature and relative humidity, Muto *et al.* found that the dew point of outdoor air remains approximately constant and that humidity depends on the air temperature [15]. A testing method based on this finding has thus been proposed to simulate the actual environment of atmospheric corrosion on stainless steel [15]. The testing method, called the constant dew point corrosion test, employs a diurnal cycle of temperature and humidity at a constant dew point temperature. It has been demonstrated that this method reproduces atmospheric corrosion well in the laboratory not only in the case of stainless steel [15] and Zn alloys [16-17] but also for aluminium and its alloys [18, 19]. Basing

on our experimental results, this testing methodology has been registered to be an international standard, ISO 16539, in 2013 [20].

The atmospheric corrosion of aluminium and its alloys was investigated in the present chapter. We focused on the applicability and reproducibility of the constant dew point corrosion tests in the field of the atmospheric corrosion of the aluminium alloys. The evaluation of the atmospheric corrosion of aluminium and its alloys was conducted from the aspects of the corrosion rates, corrosion morphology and corrosion product composition in the field exposure tests and the constant dew point corrosion tests.

2. Samples preparation and method used

In our researches, high-purity aluminium (4N Al) and two kinds of aluminium alloys, O type commercial pure aluminium (AA1100) and T6 tempered Al-Mg-Si alloy (AA6061), were tested. The chemical composition of the alloys is given in Table 1. Usually, all the samples (each with a dimension of 50 mm × 50 mm × 2 mm) were polished by emery papers. The samples were then chemically etched in a 10 wt% NaOH solution at 343 K for 30 seconds, rinsed with water, immersed in a 30 wt% HNO₃ solution at 298 K for 30 seconds, and again rinsed with water.

Field exposure tests were performed in Miyakojima (E125°19'N24°44'), Choshi (E140°45'N35°43') and Aobayama in Sendai (E140°50'N38°15'), Japan, with a map as shown in Fig. 1. The climates in Japan Weathering Testing Center (JWTC), which is 2 km far from the North Pacific Ocean, in Miyakojima are subtropical marine conditions. The climates in Choshi, which is 4 km far from the North Pacific Ocean, are typical weathering conditions as other sites in Japan. The exposure site in Aobayama campus, Tohoku University in Sendai is 6 km far from the North Pacific Ocean locating on the top of a small hill with an altitude of 100 meters.

	Si	Fe	Cu	Mn	Mg	Cr	Zn	Ti
4N Al	0.0003	0.0019	0.0004	--	0.0004	--	--	0.0003
AA1100	0.07	0.6	0.14	0.01	--	--	--	--
AA6061	0.61	0.41	0.26	0.03	1.01	0.24	0.02	0.03

Table 1. Chemical composition of 4N Al, AA1100 and AA6061 (wt%)

The tested samples were set on exposure racks facing southward at an inclination of 30° from the horizon. The two samples in each category were exposed, with one sample used for evaluating the corrosion mass losses and the other one for observing the surface and analyzing the corrosion products. Temperature, T_{air} , the relative humidity of the surrounding atmosphere, Φ_{air} , and the surface temperature of 4N Al panels, T_{Al} , were monitored by the sensors and recorded by data loggers. The accuracy of relative humidity was as high as ±2.5 % and the resolution was 0.03 %. The accuracy of temperature measurements was within ±0.2 °C, and

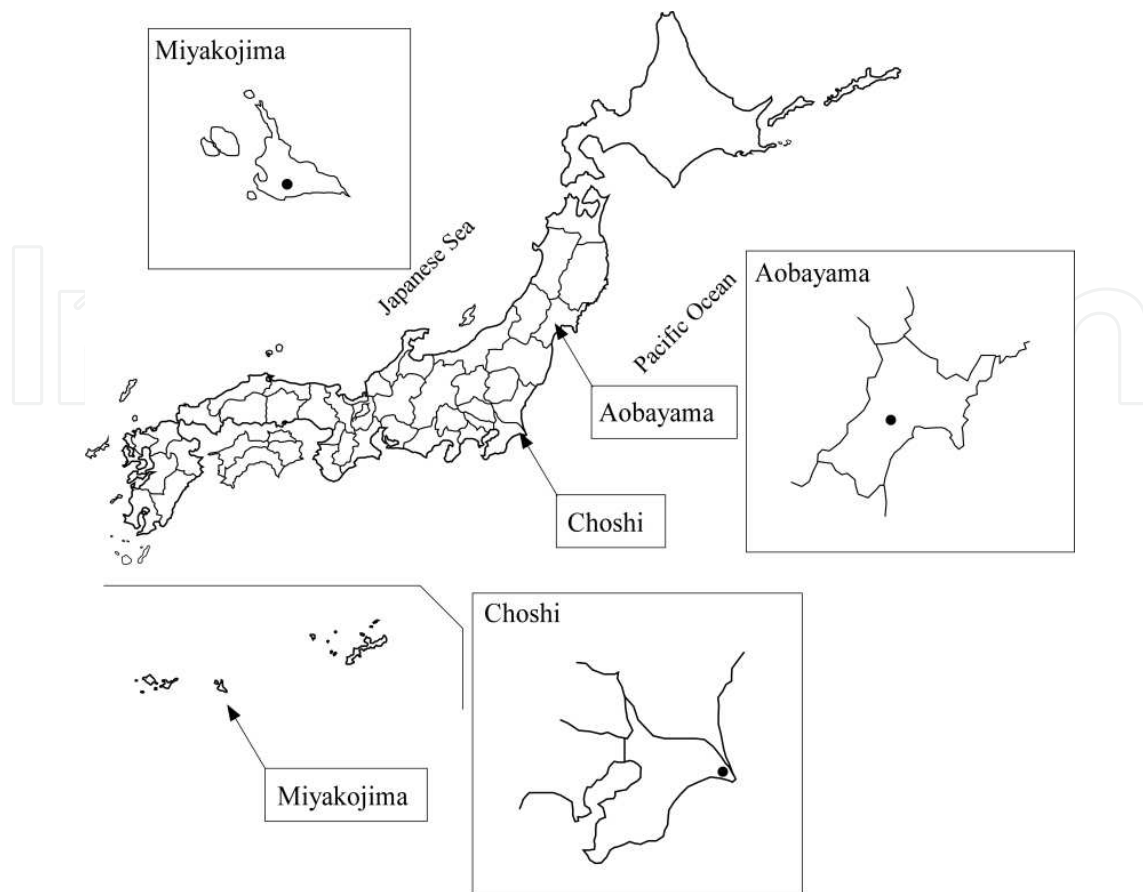


Figure 1. The exposure sites for the two-year field exposure tests performed in Japan.

the drift was less than 0.1 °C per year. The sampling interval was set at 3 minutes. The relative humidity near the 4N Al panels, Φ_{Al} , was dependent on the surface temperature of the panels, and was calculated as $\Phi_{Al} = P_{w,air} \times \Phi_{air} / P_{w,Al}$ where the saturated water vapour pressure, P_w (in Pa), is given as a function of temperature, T (in °C), by the following Sonntag Equation [21]:

$$\ln (P_w) = -6096.9385(T + 273.15)^{-1} + 21.2409642 - 2.711193 \times 10^{-2} \times (T + 273.15) + 1.673952 \times 10^{-5} \times (T + 273.15)^2 + 2.433502 \ln (T + 273.15) \quad (1)$$

The Magnus formula [21] was then used for calculating the dew point, T_d (in °C), on the Al panel surface.

$$T_d(T, \Phi) = \frac{\lambda \cdot \left(\ln \left(\frac{\Phi}{100} \right) + \frac{\beta \cdot T}{\lambda + T} \right)}{\beta - \left(\ln \left(\frac{\Phi}{100} \right) + \frac{\beta \cdot T}{\lambda + T} \right)} \quad (2)$$

where T in °C, Φ in %, $\beta=17.62$ and $\lambda=243.12$ °C.

The time of wetness (TOW) was calculated from the collected weathering data. The chloride deposition and SO₂ deposition in Miyakojima and Choshi were monitored by the JWTC. The dry gauze method, JIS Z 2382, was used for measuring the chloride deposition. This method employs a dry gauze screen (100 cm²) for sampling the chloride rather than the gauze wick (100 cm²) used in the wet candle method, ASTM G 140 and ISO 9225. The sulphation cylinder method, JIS Z 2382, was used for measuring the SO₂ deposition. This method employs a cylinder with a PbO₂-coated gauze (100 cm²) wound around it for SO₂ collection rather than the PbO₂-coated filter paper (28.26 cm²) used in the sulphation plate method, ASTM G 91 and ISO 9225. The SO₂ deposition in Aobayama was estimated from the data of SO₂ concentration in the atmosphere reported by the Japanese government's Ministry of the Environment.

The chloride deposition in Aobayama was estimated from the amount of chloride species deposited on pure Ti panels exposed at the same time. The exposed side of the Ti sample was carefully washed by deionized water to make a 100 ml solution. This solution was filtered with a 0.45 µm membrane filter and then analysed by ion chromatography (IC). Due to the washing effect of rainwater, the amount of chloride determined is somewhat different from the chloride deposition measured by the conventional method. The meteorological parameters of the three exposure sites are summarized in Table 2.

The corrosion mass loss was evaluated after the removal of the corrosion products. The corrosion products were removed by dipping test samples into a solution of phosphoric acid (50 ml/l H₃PO₄) and chromium trioxide (20 g/l CrO₃) at 90 °C for 5-10 minutes. The samples were weighed by an electric balance with a precision of 0.01 mg.

	Atmospheric data				Precipitation		
	Temperature, °C	Relative humidity %	Time of wetness, h•year ⁻¹	Rainfall, mm•year ⁻¹	pH	Cl, mg•m ⁻² • day ⁻¹	SO ₂ , mg•m ⁻² •day ⁻¹
Miyakojima	23.9	77	4350	2176.5 ¹⁾	5.12-5.16 ³⁾	56.5 ¹⁾	2.88 ¹⁾
Choshi	14.7	76	4500	1782.1 ¹⁾	4.6-5.11 ³⁾	27.4 ¹⁾	3.73 ¹⁾
Aobayama	12.7	73	2190	1303.5 ²⁾	4.6 ³⁾	5.1 ⁴⁾	1.52 ³⁾

Table 2. Summary of climate data from the field-exposure sites

1. Average values reported by Japan Weathering Test Center for the test period (Miyakojima: July, 2007-June 2008; Choshi: Aug. 2007- July 2008)
2. Reported by Japan Meteorological Agency (Sendai: Dec. 2007- Nov. 2008)
3. Reported by Japan Ministry of the Environment
4. Measured by the Ti plate method (see text)

A climatic chamber (ESPEC, SH6610) was used to perform the constant dew point corrosion tests. Each of the following environmental factors was able to be individually manipulated: the relative humidity, the temperature, the time of wetness (TOW), and the amount of airborne salt. Diluted synthetic seawater (ASTM D 1141-90) was used as a test solution to form a thin electrolyte layer with a fixed initial thickness of about 500 μm . The surface of the specimen was covered with a polyimide adhesive tape (Permacel, P-221) with the exception of a test area of 10 \times 10 mm. The chloride ion deposition on the specimen surface was adjusted to 1 g m⁻² by dropping a fixed volume of the test solution onto the test area. The dew point inside the chamber was controlled at a constant level during cyclic changes in temperature and relative humidity, as will be described in 3.2. The climatic chamber was equipped with an air circulation fan to ensure air flow so that uniform conditions inside the chamber could be maintained. After each wet-dry cycle (24 h) was completed, the specimen surface was gently rinsed with deionized water, dried in an N₂ stream, and covered with a fresh thin electrolyte layer. Although the SO₂ concentration of the chamber air was not controlled in the present study, the presence of SO₄²⁻ ions in the synthetic seawater (2.7 g/l) resulted in the condition where some SO₂ was deposited and oxidised on the sample surface. If we assume that the deposited SO₂ was completely oxidised to SO₄²⁻, it can be estimated that the chloride deposition of 1 g m⁻² of the synthetic seawater is accompanied by an SO₂ deposition of about 0.14 g m⁻².

The morphology of the samples after the corrosion tests was observed by a scanning electron microscope (SEM; Philips, XL-30). An energy dispersive X-ray spectrometer (EDX; Philips, XL-30) was employed to analyze the elemental distributions at local parts of the samples exposed for 3 and 12 months at the three different sites. The samples used for cross-sectional observation were embedded into epoxy resin and finely polished by a 1 μm diamond paste.

A Fourier transform infrared spectrometer (FT-IR; JASCO, FT-IR 4200) was used to identify the corrosion products. The assignment of the characteristic peaks was on the basis of the spectra measured from analytical grade Al(OH)CO₃ and Al(OH)₃ powder. Basic aluminium sulphate (Al_x(OH)_ySO₄_nH₂O) was made in the laboratory and analyzed by FT-IR. The characteristic peaks of dawsonite (NaAlCO₃(OH)₂) were assigned by referring to the data in the literature.

3. Important findings

3.1. Characteristics of atmospheric corrosion in the field exposure tests

3.1.1. Real-time changes in temperature, relative humidity of the ambient atmosphere and surface temperature of specimens

The synchronous changes of four parameters, i.e. the relative humidity of the ambient air (Φ_{air}), the relative humidity of the tested 4N Al samples (Φ_{Al}), the temperature of the ambient air (T_{air}) and the temperature of the tested 4N Al samples (T_{Al}) between July 18, 2007 and July 25, 2007 in Miyakojima are shown in Fig. 2a. In the daytime, the temperature of the samples increased due to their exposure to sunshine. While the temperature decreased from radiation

cooling in the night, the relative humidity increased and a dew film consequently formed on the surface. The change in relative humidity was inversely proportional to the temperature change. However, the collected relative humidity and temperature data shows that the dew point of both the atmosphere and the samples remains constant for short-term periods. This can be seen, in Fig. 1b, where experimental Φ_{Al} vs T_{Al} plots are compared with theoretical Φ - T curves for different dew point temperatures. These results are consistent with the findings of earlier studies reported by Muto *et al.* [15]. In addition, the time of wetness was 49.7% of the calendar time in Miyakojima, 51.4% in Choshi and 25.0% in Aobayama, respectively. The weathering data show that the long-term dew point varied with both the exposure time and the seasons, as shown in Fig. 3. The average dew point changed on a large scale, from 5.5 to 28.4 °C in Miyakojima, from -10.1 to 24.6 °C in Choshi and from -13.0 to 23.6 °C in Aobayama. However, the short-term dew point remains constant with a drift of 5 °C.

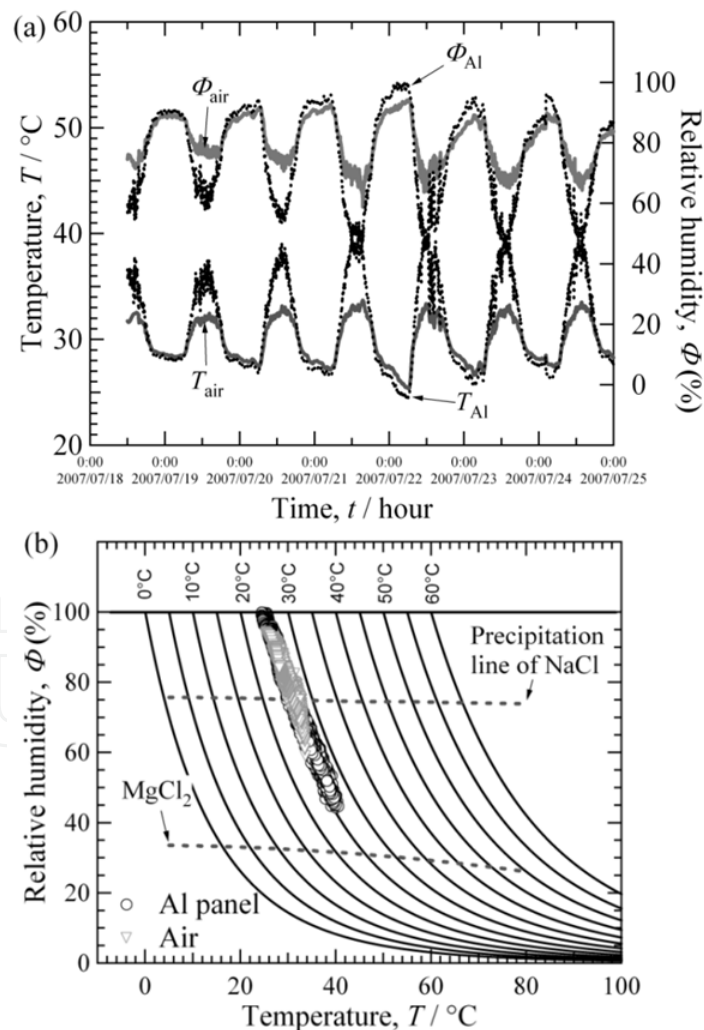


Figure 2. Changes in relative humidity, Φ and temperature, T , of the ambient atmosphere and 4N aluminium (a) and Φ vs. T plot (b) in Miyakojima from July 18th to July 25th, 2007. [18]

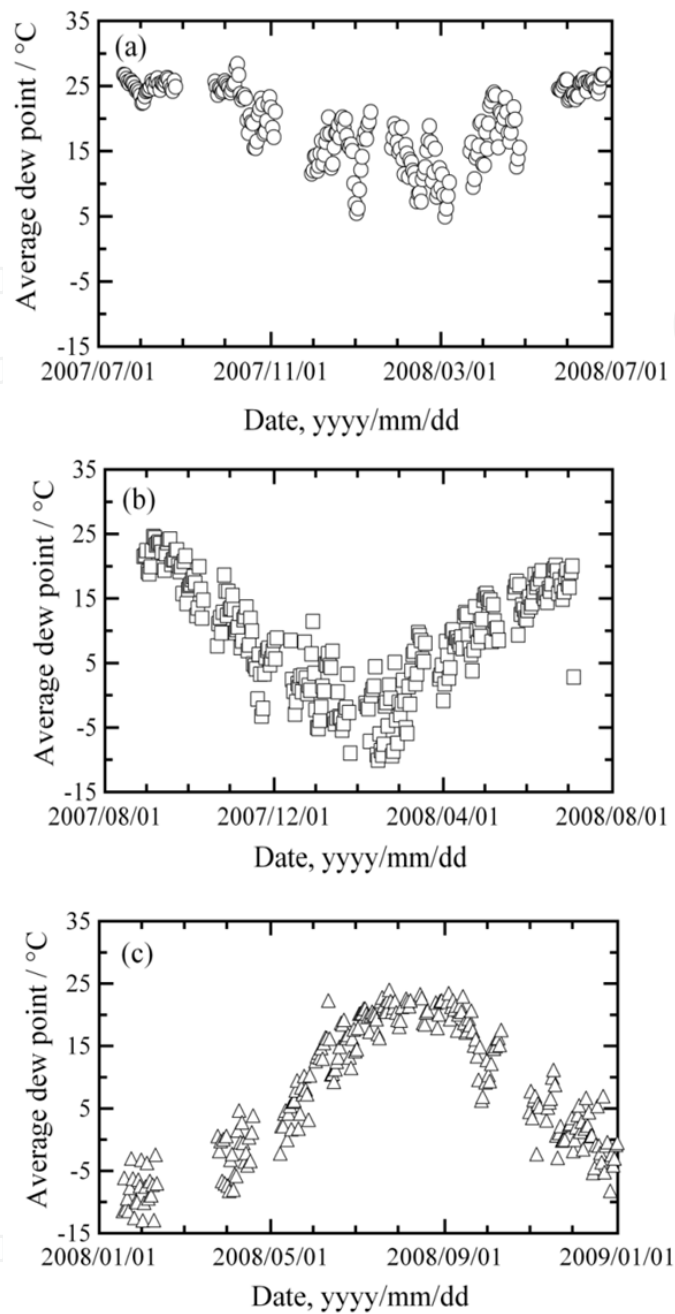


Figure 3. Changes in the dew point in Miyakojima (a), Choshi (b) and Aobayama (c) during the one year of exposure tests. [18]

3.1.2. Corrosion mass loss

The corrosion mass losses of aluminium and its alloys exposed at the three different sites are plotted against exposure time in Fig. 4. As described in the experimental section, the corrosion mass loss for each exposure period was determined by just one sample, and thus some degree of uncertainty can be expected. Though corrosion mass losses increased with exposure time, their increasing rate slowed down with the lapse of time. Corrosion mass losses, ΔW , as a

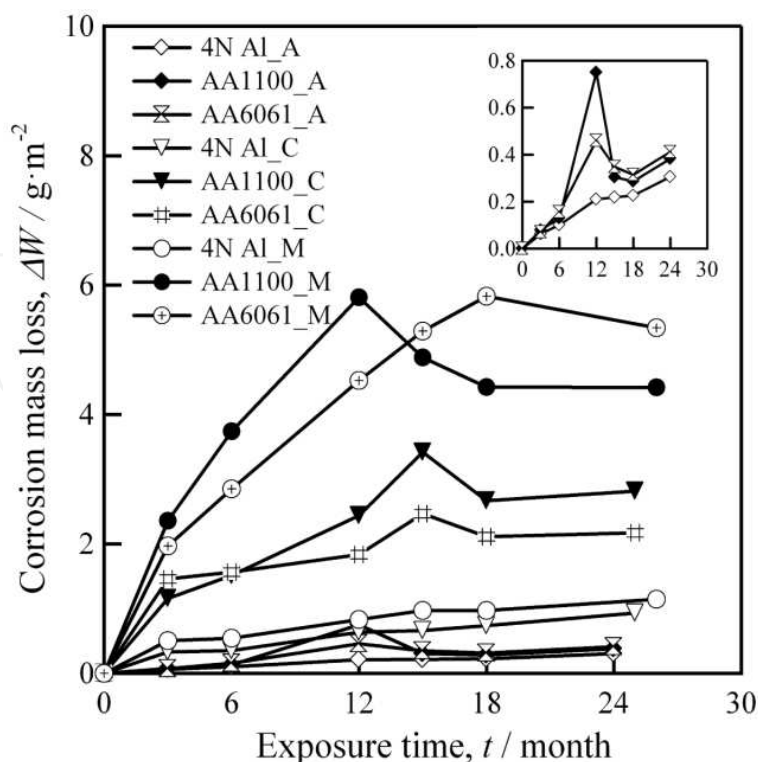


Figure 4. Corrosion mass losses of 4N Al, AA1100 and AA6061 at the three exposure sites as a function of exposure time. The magnified zone at the top right shows the corrosion mass loss in Aobayama. (A: Aobayama; C: Choshi; M: Miyakojima). [18]

function of the exposure time, t , were well yielded to general damage functions in the form of $\Delta W = A \times t^n$, where A and n are constants [22, 23]. Most of the n values of the fitted damage functions were close to 0.5, indicating that the rate of atmospheric corrosion is controlled by a diffusion process through the insoluble corrosion product which functions as an unperturbed layer. Corrosion resistance increased in the following order: 4N Al > AA6061 > AA1100. Meanwhile, the order of the corrosiveness of the exposure sites is ranked as Miyakojima > Choshi > Aobayama. The corrosion mass losses of aluminium and its alloys depended not only on the exposure time but also on the meteorological parameters of the exposure sites. To a greater or less extent, the n value also strongly depends on such environmental factors as the deposition rate of sulphur dioxide and sea salts, relative humidity and temperature. The corrosion rates of aluminium and its alloys were suppressed during the field exposure, particularly after the first 3 months.

3.1.3. Corrosion morphology

Both AA1100 and AA6061 suffered from tarnishing and pitting corrosion observable to the naked eye. Some parts of the surface remained stable with a complete absence of local attacks even after 12 months of exposure. The roughness of the surface and the ratio of the corroded areas increased with the exposure time. The 4N Al in three sites presented excellent corrosion resistance even though some micro-sized pits were detected.

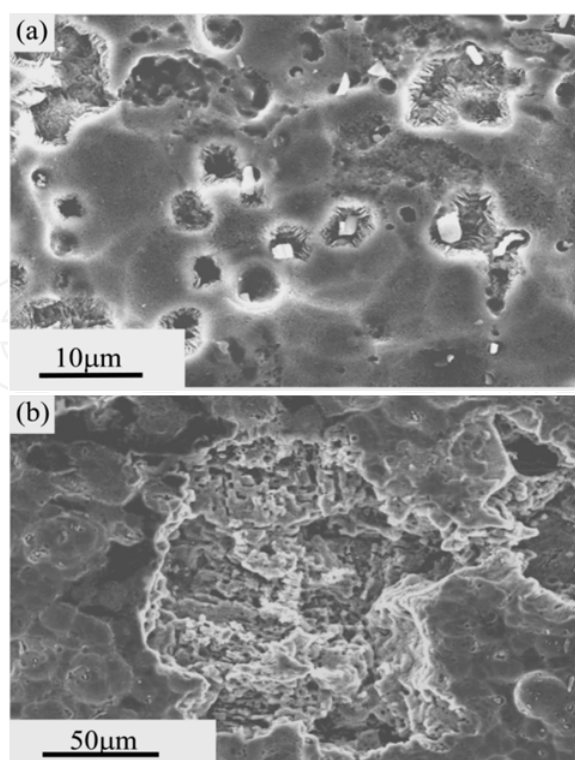


Figure 5. Corrosion morphology of AA1100 exposed in Miyakojima for 3 (a) and 12 (b) months, respectively. [18]

Figure 5 shows the corrosion morphology of AA1100 exposed in Miyakojima for 3 and 12 months. The sample was observed by SEM after the removal of the corrosion products. After 3 months of exposure, pits were formed around some particles, such as inclusions, second phases or the intermetallics, as shown in Fig. 5a. Some pits grew up to several tenths of micrometers after 12 months of exposure, as shown in Fig. 5b. As exposure was extended, some more seriously corroded sites formed visible pits of up to a hundred micrometers in size.

3.1.4. Corrosion products

The corrosion products of aluminium and its alloys exposed in the fields were porous and rich in cracks. It was confirmed that corrosion primarily attacked the grain boundaries of AA6061 and a high-facet crystallographic morphology was frequently observed, which is typical for aluminium dissolution under an open circuit potential [24, 25]. In addition, the corrosion product cups were usually circular and typical of those which generate around such cathodic intermetallics as Al_3Fe and Al_2Cu in AA1100 [26, 27]. These intermetallics Al_3Fe and Al_2Cu usually have more noble corrosion potentials in comparison to pure Al. Al_3Fe and Al_2Cu particles usually act as cathodes to form micro-coupling cells with adjacent Al matrix, and trigger the dissolution of surrounding Al matrix of intermetallics to form the trenches just as shown in Fig. 5a.

The corrosion products were analyzed by energy dispersive X-ray spectrometry (EDX) and FT-IR. The EDX analysis showed that the surface regions of the corrosion products consisted of various elements, including Al, Na, O, S, and Cl, after aluminium and its alloys were exposed

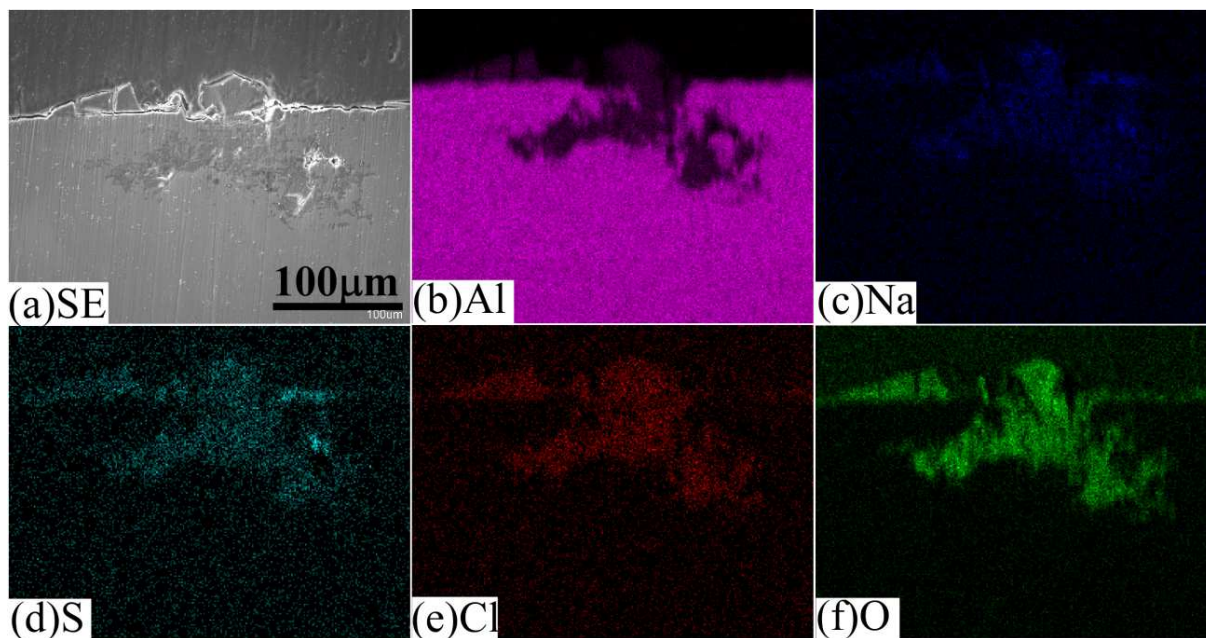


Figure 6. Cross-sectional morphology (a) and X-ray mapping of Al (b), Na (c), S (d), Cl (e) and O (f) obtained from 3-month exposed AA1100 in Miyakojima. [18]

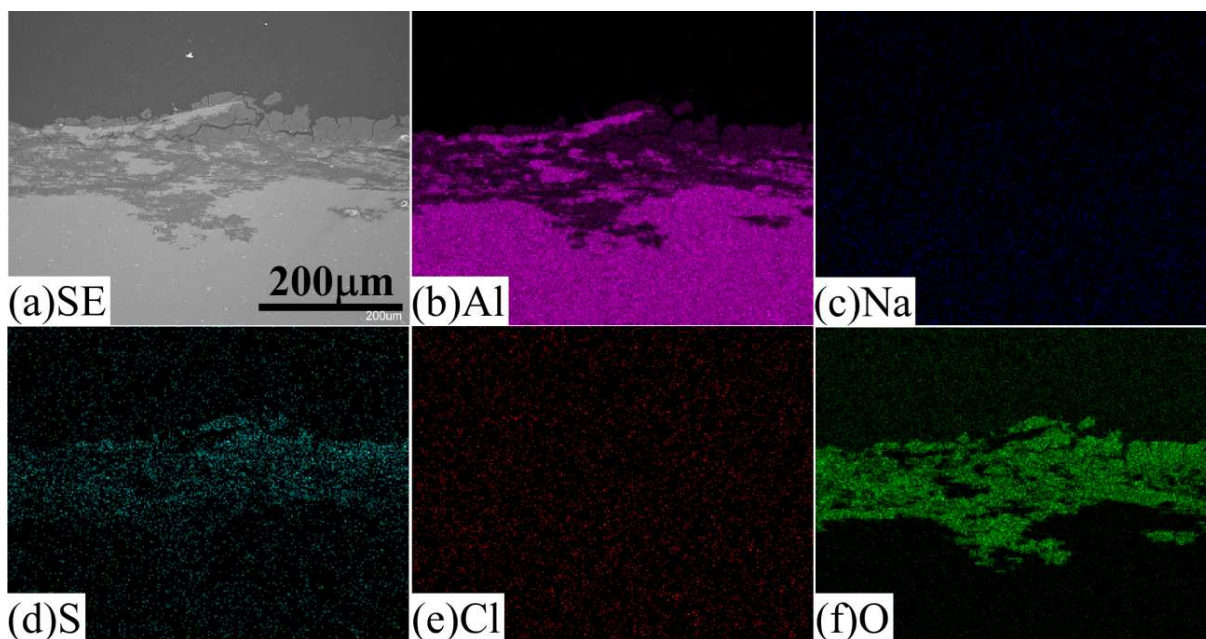


Figure 7. Cross-sectional morphology (a) and X-ray mapping of Al (b), Na (c), S (d), Cl (e) and O (f) obtained from 12-month exposed AA1100 in Miyakojima. [18]

in Miyakojima for 3 months. However, as the exposure time increased up to 12 months, the main elements distributed on the surface of the corrosion products were Al, S, and O. Further analysis was conducted to obtain cross-sectional elemental distribution maps, and the results are shown in Fig. 6 and 7 for AA1100 exposed in Miyakojima for 3 and 12 months, respectively. The data in Fig. 6 indicates that the corrosion products formed after 3 months of exposure

consisted mainly of Al, Na, S, C, Cl and O. Chlorine- and sulphur-containing species were distributed inside the pits. However, the corrosion products formed after 12 months of exposure were composed of Al, O and S, as shown in Fig. 7. No signals were detected from many of the elements in the corrosion products after 3 months, notably for Na, Mg, Cl and C, indicating that none of these chemical species accumulated in the corrosion products, perhaps because the rain washes away soluble species once they are deposited.

Further analysis of the corrosion products was performed by FT-IR. Fig. 8a shows the FT-IR spectra of corrosion products formed on AA1100 after 3, 12 and 26 months of exposure in Miyakojima. Figure 8b shows the spectra of analytic grade basic aluminium carbonate, aluminium hydroxide and lab-synthesized basic aluminium sulphate. For the spectrum of dawsonite and also for that of basic aluminium sulphate, we referred to the literature [28-32]. The characteristic adsorption peaks of basic aluminium sulphate are 1135 (ν_3 SO₄ asymmetric stretching), 980 (ν_1 SO₄ symmetric stretching), 715 (ν_4 SO₄ in-plane deformation), 610 (ν_4 SO₄), 566 (ν_2 SO₄ out-of-plane deformation SO₄) and 450 (ν_2 SO₄) cm⁻¹ [28-30, 32]. The characteristic adsorption peaks of dawsonite are 3274, 1560 and 1390 (doublet peaks, ν_3 CO₃ asymmetric stretching) cm⁻¹, 854 (ν_2 CO₃ out-of-plane deformation) cm⁻¹ and 540-480 cm⁻¹ (a broad peak) [31]. As shown in Fig. 8 (b), the spectrum of Al(OH)CO₃ included several peaks, such as 1560, 1390 cm⁻¹ (doublet peaks), 2464 and 2603 cm⁻¹ (doublet peaks), 1103 (ν_1 CO₃ symmetric stretching), 980 cm⁻¹ (δ -OH stretching), 854 cm⁻¹ (ν_2 CO₃ out-of-plane deformation) and 540-480 cm⁻¹ (a broad peak). The peaks of dawsonite frequently overlapped with those of basic aluminium carbonate at different positions. After 3 months of exposure in Miyakojima, a small doublet peak around 2500 cm⁻¹ appeared which can be assigned to the CO₃²⁻ species, proving that the corrosion products in the surface region consisted of either basic aluminium carbonate (Al(OH)CO₃) or dawsonite, and the broad peaks in the low wavenumber region were assigned to sulphate ions. However, the EDS elemental maps (Fig. 7) show the coexistence of Na in the corrosion products, suggesting that the dawsonite species were the main carrier of the carbonate ions. With increasing exposure time, the doublet peak of carbonate became weaker and the peaks in the low wavenumber region became stronger, which can be attributed to the incorporation of sulphate ions. Moreover, the stronger intensity of the ν_3 SO₄ asymmetric stretching peak around 1135 cm⁻¹ indicates an increase of the basic aluminium sulphate in the corrosion product layer. Generally, if field-exposed samples yield a strong and broad peak in the range of 3200 to 3600 cm⁻¹, it is assigned to the O-H stretching mode, and a medium peak at 1640 cm⁻¹ was assigned to the H-O-H bending mode. The latter peak indicates the presence of free water combined with the corrosion products. The FT-IR spectra demonstrated that the existence of carbon and sulphur in the form of CO₃²⁻ and SO₄²⁻. It was concluded that the corrosion products which formed in the first three months were aluminium hydroxide, basic aluminium sulphate, basic aluminium chloride and Na-containing basic aluminium carbonate. After 12 months of exposure, the basic aluminium carbonate and basic aluminium chloride content decreased; as a result, aluminium hydroxide and basic aluminium sulphate became the main constituents.

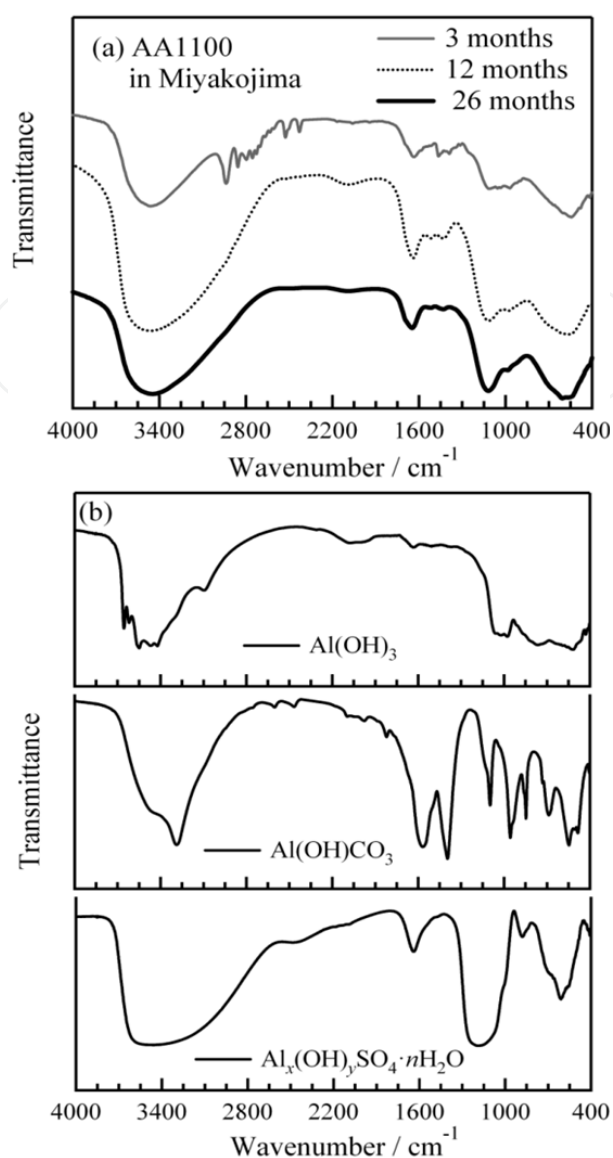


Figure 8. FT-IR spectra of corrosion products formed on AA1100 after 3, 12, and 26 months of exposure in Miyakojima (a) and reference spectra of aluminium hydroxide, basic aluminium carbonate and lab-made basic aluminium sulphate (b). [18]

3.2. Characteristics of atmospheric corrosion in the constant dew point corrosion tests

The practical dew point in Miyakojima from July 18, 2007 to July 25, 2007 in the middle of the summer season was about 26 °C in Fig. 2b. In order to simulate the practical atmospheric conditions in Miyakojima in summer season, the relative humidity and temperature were controlled according to the patterns shown in Fig. 9a, and the corresponding iso-dew point line is shown in Fig. 9b. The dew point of the pattern was maintained at 28 °C. The time of wetness was about 60%. The single cycle was 24 hours, and consisted of wetting (condensation) and drying (evaporation) stages. The chloride deposition was set at a relatively high level of 1 g·m⁻² to simulate a severe coastal site.

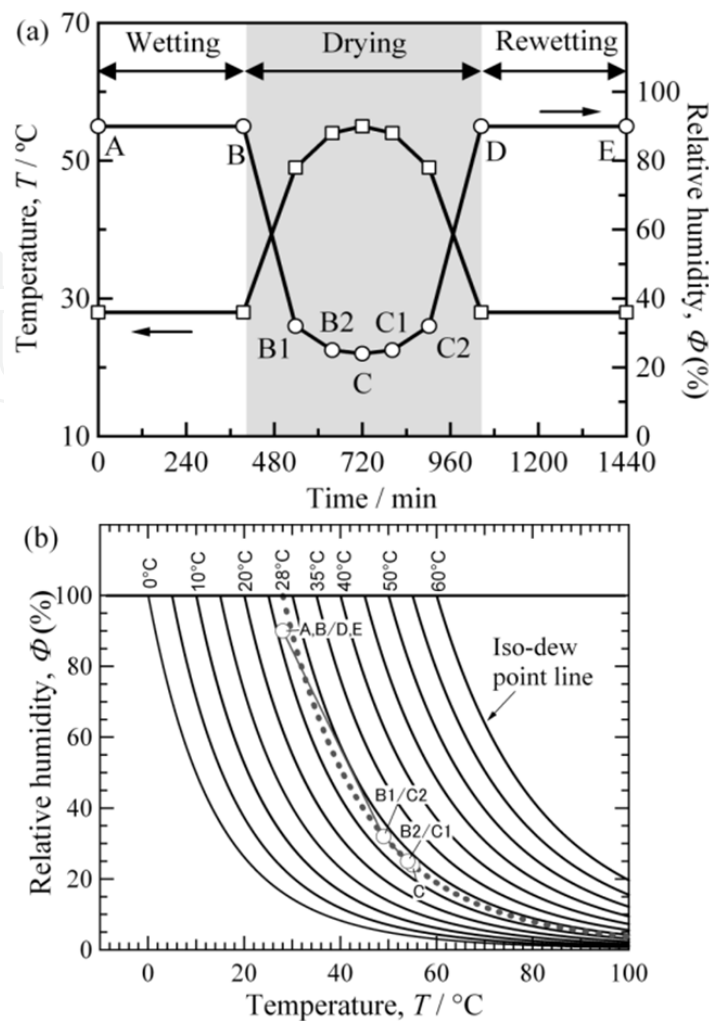


Figure 9. Real-time change pattern of relative humidity, Φ and temperature, T , during the constant dew point corrosion test with a dew point of 28 °C (a) and corresponding Φ vs. T plot (b). [18]

3.2.1. Corrosion mass loss

The corrosion mass losses of aluminium and its alloys exposed in the constant dew condition are shown in Fig. 10. The tests were repeated two or three times for each alloy. The averaged values and the maximum and minimum values of mass losses were determined and are shown in Fig. 10 as legends and error bars, respectively.

In a similar manner as the field exposure test, the mass loss increases as the number of test cycles increases, and is expressed in the form of the general damage function. The comparison of the fitted parameters of the general damage functions obtained from the constant dew point corrosion tests was conducted between the field exposure tests. The experimental data collected from the laboratory tests were in good agreement with those collected from the field experiments. A comparison of the two sets of results indicates that the corrosion mass loss of aluminium and its alloys after the constant dew point corrosion tests showed almost the same tendencies as the field exposure tests. The n value was close to 0.5, indicating that the corrosion product layer functioned as a barrier for diffusion. Nevertheless, the constant dew point

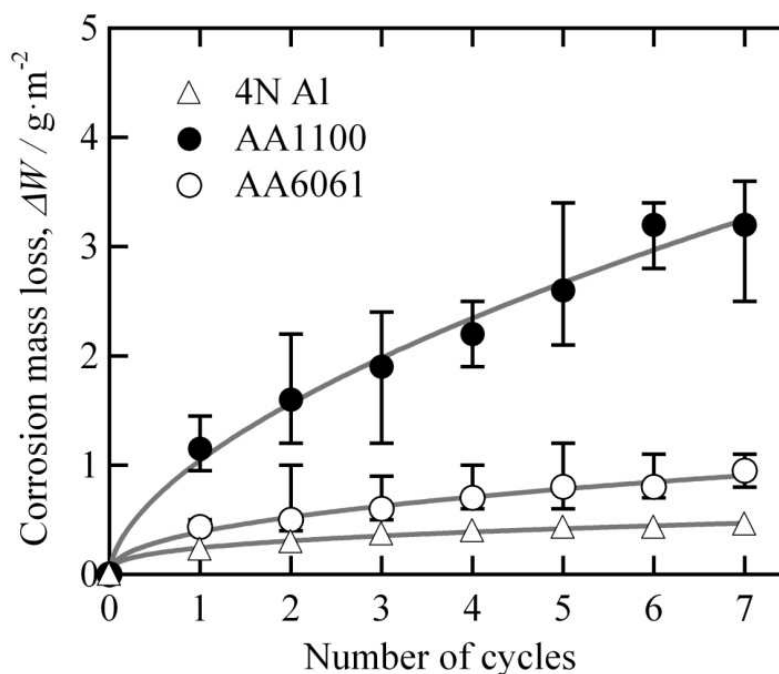


Figure 10. Corrosion mass losses of 4N Al, AA1100 and AA6061 after constant dew point tests as a function of the cycle number. [18]

corrosion test accelerated the corrosion. When the corrosion mass loss value of AA1100 after 7 cycles, $3.22 \text{ g}\cdot\text{m}^{-2}$, is put into the fitted damage function for the same alloy exposed in Miyakojima, $\Delta W = 4.35 \times t^{0.48}$, it is found that the constant dew point test of 7 cycles (7 days) corresponds to the field exposure test for 104 days in Miyakojima. This indicates that the constant dew point test accelerates the corrosion of AA1100 by a factor of about 15. In the same manner as for AA1100, the acceleration ratio of the constant dew point test with respect to the field exposure test in Miyakojima is estimated to be about 2 and 14 for AA6061 and 4N Al, respectively. Except for AA6061, the constant dew point test for a week corresponds to the field exposure test for about 3 months in Miyakojima. Atmospheric corrosion does not proceed continuously but occurs during the period when the metal surface is covered with a thin corrosive electrolyte layer. The samples do not always meet this corrosion condition in actual atmospheric corrosion environments, but a corrosive electrolyte layer is formed for in every wet-dry cycle of the constant dew point test. Therefore, the constant dew point test accelerates the corrosion.

3.2.2. Corrosion morphology

Macroscopically, the main forms of corrosion attacks seem to be pitting corrosion and tarnishing. The corrosion products exhibited a porous, cracked state. Cups of corrosion products formed on the surface as they did in some cases in the field. Trenches formed around some particles after the first cycle of exposure (Fig. 11a). The pit formed in the substrate with similar shapes as those formed in the field (Fig. 11b). The localized corrosion gradually grew deeper and wider. The corrosion behaviour was influenced by microstructure. The existence

of the cathodic intermetallics (Al_3Fe and Al_2Cu) in AA1100 and AA6061, and sacrificial anodic intermetallics (Mg_2Si) in AA6061 caused preferential electrochemical dissolution in the form of micro-coupling cells [33]. Pits formed on the aluminium alloys around cathodic intermetallics of several micrometers in size, which indicated that the localized corrosion initiated around intermetallics [33-35]. Some pits grew to several hundreds of micrometers in size after short exposure. The corrosion morphologies, including the structure of the corrosion products, the corrosion patterns and the shapes of the cups and pits produced, were similar with those visible in samples from the field.

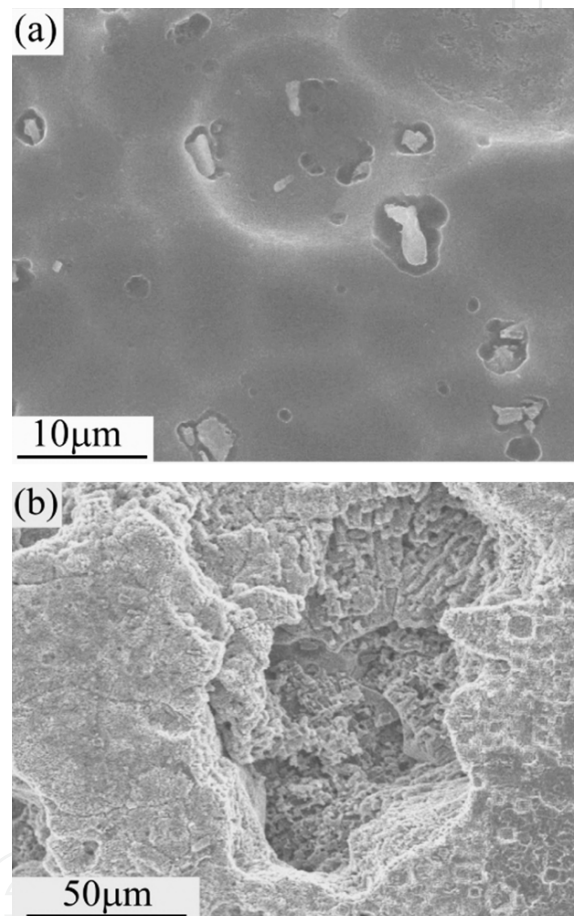


Figure 11. Corrosion morphology of AA1100 exposed for 1 (a) and 7 (b) cycles of constant dew point corrosion tests with a chloride deposition of $1 \text{ g} \cdot \text{m}^{-2}$ and a dew point of $28 \text{ }^\circ\text{C}$. [18]

3.2.3. Corrosion products

The element distribution profiles inside the pits formed after 7 cycles of constant dew point corrosion tests are shown in Fig. 12. While there was Cl inside the pits, and enriched Cl at the bottom of the pits, sulphur was highly concentrated in the outermost layer of the corrosion products. Generally, the element distribution profiles were similar with those obtained from 3-month exposed AA1100.

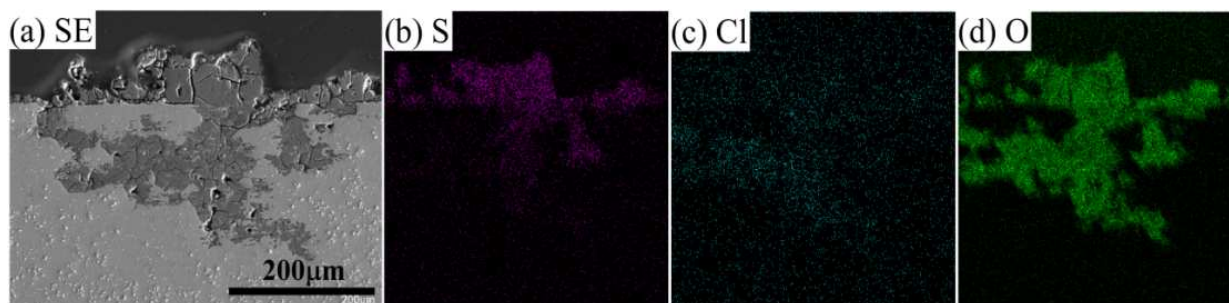


Figure 12. Cross-sectional morphology (a) and X-ray mapping of S (b), Cl (c) and O (d), obtained from AA1100 after 7 cycles of exposure in the constant dew point test with a chloride deposition of $1 \text{ g} \cdot \text{m}^{-2}$ and a dew point of $28 \text{ }^\circ\text{C}$. [18]

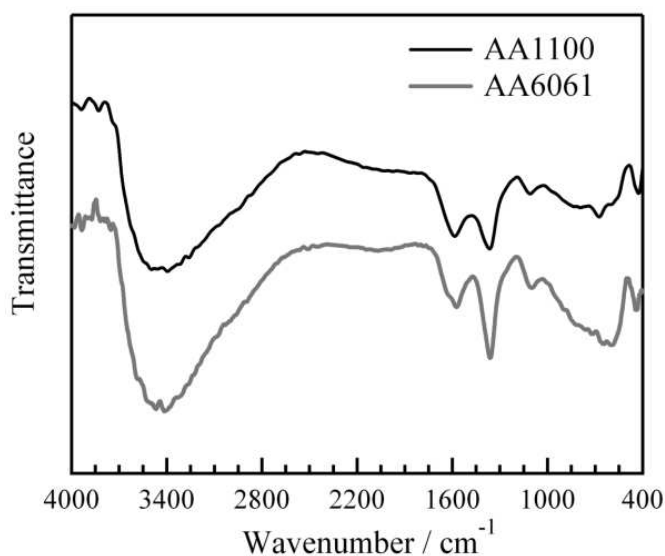


Figure 13. FT-IR spectra of corrosion products on AA1100 and AA6061 after 7 cycles of the constant dew point test with a chloride deposition of $1 \text{ g} \cdot \text{m}^{-2}$ and a dew point of $28 \text{ }^\circ\text{C}$. [18]

Figure 13 shows the FT-IR spectrum of the corrosion products formed on AA1100 and AA6061 after 7 days of constant dew point corrosion tests in the laboratory. The corrosion products include carbonate ions ($1390, 1560 \text{ cm}^{-1}$), sulphate ions ($1085, 640, \text{ and } 450 \text{ cm}^{-1}$) and water (1640 cm^{-1}). This is similar to the FT-IR results of field-exposed aluminium and its alloys. Both EDX and FT-IR analysis demonstrated that the corrosion products consisted mainly of basic aluminium sulphate, basic aluminium chloride, aluminium hydroxide and basic aluminium carbonate. The washing effect of rain is difficult to reproduce in a short time. Due to limited exposure time, the amount of basic aluminium sulphate and aluminium hydroxide in the corrosion product layer was considerably lower than that formed in the field samples with more than 12 months of exposure. The other corrosion products were close to those from the initial case of field exposure tests.

The observed data of the dew point change in the surrounding atmosphere and at the surface showed that the short-term dew point remained at a constant level. The dew point is associated with the heat capacity of the materials and the ratio of water vapour and dry air. Heat flux in

a closed system is mainly determined by the evaporation (heating) and condensation (cooling) of the water content in the air. Though the practical open environment cannot be regarded as a closed system, at least for short periods of time, the surrounding region of the samples can be considered a closed system, where the heat flux and the flow of humid air remain stable and move freely around the samples [15, 36]. Consequently, the heat flux around the exposed samples remains constant, which results in the occurrence of the constant dew point [36-38]. The constant dew point corrosion testing model therefore has a more concrete base than other simulation methodologies in terms of its ability to model the practical conditions.

The accumulation of the sulphate ions in the localized corroded sites was observed in both the field exposure tests and the constant dew point tests indicated by the element mapping data. Due to effects of daily alternations of the wet-dry surface state and washing of raining, very few highly soluble chlorine-containing species accumulated inside the pits [5, 39]. On the other hand, ten times more sulphate ions accumulated than chloride ions [6, 40, and 41]. With increasing exposure time, such compounds as basic aluminium carbonate and basic aluminium chloride were washed away by rain while the insoluble ones, such as aluminium hydroxide and basic aluminium sulphate, remained as long-term stable corrosion products. The constant dew point test with 7 cycles is incapable of reproducing the process completely due to the limited exposure time. Consequently, strong peaks of carbonate were detected in the lab-exposed samples. Based on the surface morphology, corrosion mass loss and chemical compounds, we were able to reproduce the initial stage of the atmospheric corrosion of aluminium and its alloys by using the constant dew point test over the initial period.

4. Conclusion

In order to examine whether the constant dew point corrosion test can appropriately reproduce the atmospheric corrosion of aluminium alloys, corrosion tests were performed on AA1100, AA6061 and 4N Al under the cyclic wet-dry conditions at the constant dew point of 28 °C and with the chloride deposition of 1 g·m⁻², which simulated marine atmospheric environments in the summer season in Japan. It was found that the corrosion mass loss increased as the number of cycles increased in accordance with a power-law formula. The corrosion pattern after the 7-cycle test was pitting, and the corrosion products consisted of basic aluminium sulphate, basic aluminium chloride, aluminium hydroxide, and basic aluminium carbonate. The corrosion rates, corrosion morphology and corrosion product composition were similar to those observed on the samples exposed for a few months in Miyakojima, a typical coastal site. The constant dew point corrosion test, therefore was shown capable not only of reproducing the atmospheric corrosion of aluminium, but also of accelerating it.

Acknowledgements

This research is partially supported by the Ministry of Education, Culture, Sports, Science, and Technology (MEXT) through a Grant-in-Aid for Young Scientists (B) under Grant No. 24760567

and Grant-In-Aid for Science Research in a Priority Area on “Research and Development Project on Advanced Materials Development and Integration of Novel Structured Metallic and Inorganic Materials”.

Author details

Zhenhua Dan, Izumi Muto and Nobuyoshi Hara

Department of Materials Science, Tohoku University, Sendai, Japan

References

- [1] Hatch JE. Aluminium: Properties and Physical Metallurgy. In: American Society of Metals, Metals Park, OH, 1984, p2-24.
- [2] Davis JR. ASM Specialty Handbook: Aluminium and Aluminium Alloys. In: ASM International, Metals Park, OH, USA, 1993, p8-55.
- [3] Green JAS. Aluminium Recycling and Processing for Energy Conservation and Sustainability. ASM International, Metals Park, OH, USA, 2007.
- [4] McGeary FL., Summerson TJ., Ailor WH. Atmospheric Exposure of Nonferrous Metals and Alloys-Aluminium: Seven-Year Data, Metal Corrosion in the Atmosphere, ASTM STP 435, American Society for Testing and Materials, 1968. p141-174.
- [5] Friel JJ. Atmospheric Corrosion Products on Al, Zn, and AlZn Metallic Coatings. Corrosion 1986;42:422-6.
- [6] Graedel TE. Corrosion Mechanisms for Aluminum Exposed to the Atmosphere. Journal of Electrochemical Society 1989;136: 204C-12C.
- [7] Vera R., Delgado D., Rosales BM. Effect of Atmospheric Pollutants on the Corrosion of High Power Electrical Conductors: Part 1. Aluminium and AA6201 Alloy. Corrosion Science 2006;48: 2882-900.
- [8] de la Fuente D., Otero-Huerta E., Morcillo M. Studies of Long-term Weathering of Aluminium in the Atmosphere. Corrosion Science 2007;49:3134-48.
- [9] Blücher DB., Lindström R., Svensson JE., Johansson LG. The Effect of CO₂ on the NaCl-Induced Atmospheric Corrosion of Aluminum. Journal of Electrochemical Society 2001;148:B127-31.
- [10] Lyon SB., Thompson GE., Johnson JB. Accelerated Atmospheric Corrosion Testing Using a Cyclic Wet/Dry Exposure Test: Aluminum, Galvanized Steel, and Steel. Corrosion 1987;43: 719-26.

- [11] Shi Y., Zhang Z., Su J., Cao F., Zhang J. Electrochemical Noise Study on 2024-T3 Aluminium Alloy Corrosion in Simulated Acid Rain under Cyclic Wet-dry Condition. *Electrochimica Acta* 2006;51:4977-86.
- [12] El-Mahdy GA., Kim KB. AC Impedance Study on the Atmospheric Corrosion of Aluminium under Periodic Wet-dry Conditions. *Electrochimica Acta* 2004;49:1937-48.
- [13] Deflorian F., Rossi S., Prosseda S. Improvement of Corrosion Protection System for Aluminium Body Bus Used in Public Transportation. *Materials and Design* 2006;27:758-69.
- [14] Nazarov A., Thierry D. Rate-determining Reactions of Atmospheric Corrosion. *Electrochimica Acta* 2004;49:2717-24.
- [15] Muto I., Sugimoto K. Modeling of Atmospheric Corrosion Environments and Its Application to Constant Dew-point Corrosion. *Zairyo-to-Kankyo* 1998;47:519-27.
- [16] Muto I., Yoshida H., Ogawa H., Hara N. Effect of Alloying Elements on Atmospheric Corrosion Behavior of Zinc Die-casting Alloys. *Journal of Japan Institute of Metals* 2008;72: 337-46.
- [17] Shinozaki J., Muto I., Ogawa H., Hara N. Effects of Third Element Addition on Atmospheric Corrosion Resistance of Zinc-aluminum Die-cast Alloys. *Journal of Japan Institute of Metals* 2009;73:533-41.
- [18] Dan ZH., Takigawa S., Muto I., Hara N. Applicability of Constant Dew Point Corrosion Tests for Evaluating Atmospheric Corrosion of Aluminium Alloys. *Corrosion Science* 2011; 53: 2006-14.
- [19] Dan ZH., Muto I., Hara N. Effects of Environmental Factors on Atmospheric Corrosion of Aluminium and Its Alloys under Constant Dew Point Conditions, *Corrosion Science* 2012; 57: 22-9.
- [20] Muto I. Corrosion of Metals and Alloys- Accelerated Cyclic Corrosion Tests with Exposure to Synthetic Ocean Water Salt-Deposition Process-“Dry” and “Wet” Conditions at Constant Absolute Humidity. *International standard (ISO) 2013(E);16539:1-19*
- [21] Sonntag D. Important New Values of the Physical Constants of 1986, Vapour Pressure Formulations Based on the ITS-90, and Psychrometer Formulae. *Journal of Meteorology*1990;40:340-4.
- [22] Dean SW., Anthony WH. Atmospheric Corrosion of Wrought Aluminium Alloys during a Ten-year Period, Degradation of Metals in the Atmosphere, ASTM STP 965, in: S.W. Dean and T. S. Lee (Eds.), American Society for Testing and Materials, Philadelphia, 1988, pp. 191-205.
- [23] Kobus J. Long-term Atmospheric Corrosion Monitoring. *Materials and Corrosion* 2000;51:104-8.

- [24] Baumgärtner M., Kaesche H. Aluminum Pitting in Chloride Solutions: Morphology and Pit Growth Kinetics. *Corrosion Science* 1990;31:231-6.
- [25] Guillaumin V., Mankowski G. Localized Corrosion of 6056 T6 Aluminium Alloy in Chloride Media. *Corrosion Science* 2000;42:105-25.
- [26] Birbilis N., Buchheit RG. Investigation and Discussion of Characteristics for Intermetallic Phases Common to Aluminum Alloys as a Function of Solution pH. *Journal of Electrochemical Society* 2008;155:C117-26.
- [27] Park JO., Paik CH., Huang YH., Alkire RC. Influence of Fe-Rich Intermetallic Inclusions on Pit Initiation on Aluminum Alloys in Aerated NaCl. *Journal of Electrochemical Society* 1999;146:517-23.
- [28] Contreras CA., Sugita S., Ramos E. Preparation of Sodium Aluminate from Basic Aluminum Sulfate. *Advances in Technology of Materials and Materials Processing Journal* 2006;8:122-35.
- [29] Kloprogge JT., Geus JW., Jansen JBH., Seykens D. Thermal Stability of Basic Aluminum Sulphate. *Thermochimica Acta* 1992; 209:265-76.
- [30] Kloprogge JT., Frost RL. The Dehydroxylation of Basic Aluminum Sulfate: An Infrared Emission Spectroscopic Study. *Thermochimica Acta* 1998;320:245-52.
- [31] Yalfani MS., Santiago M., Pérez-Ramírez J. In Situ Studies During Thermal Activation of Dawsonite-type Compounds to Oxide Catalysts. *Journal of Material Chemistry* 2007;17:1222-29.
- [32] Bishop JL., Murad E. The Visible and Infrared Spectral Properties of Jarosite and Alunite. *American Mineralogist* 2005;90:1100-7.
- [33] Wong KP., Alkire RC., Local Chemistry and Growth of Single Corrosion Pits in Aluminium, *Journal of Electrochemical Society* 137 (1990) 3010-5.
- [34] Vermilyea DA. Concerning the Critical Pitting Potential. *Journal of Electrochemical Society* 1971;118:529-31.
- [35] Tanem BS., Svenningsen G., Mädaalen J. Relations between Sample Preparation and SKPFM Volta Potential Maps on an EN AW-6005 Aluminium Alloy. *Corrosion Science* 2005;47:1506-19.
- [36] Dean SW., Reiser DB., Time of Wetness and Dew Formation: A Model of Atmospheric Heat Transfer, in: Kirk WW., Lawson HH. (Eds.), *Atmospheric Corrosion*, ASTM STP 1239, American Society for Testing and Materials, Philadelphia, PA, 1995, p3-10.
- [37] Cole IS., Holgate R., Kao P., Ganther W. The Rate of Drying of Moisture from a Metal Surface and its Implication for Time of Wetness. *Corrosion Science* 1995;37:455-65.

- [38] Incropera FP., DeWitt DP. Fundamentals of Heat and Mass Transfer (3rd Edn.), John Wiley and Sons, New York, 1990.
- [39] Foley RT., Nguyen TH. Chemical Nature of Aluminium Corrosion. Journal of Electrochemical Society 1982;129:464-7.
- [40] Adams F., Rawajfih Z. Basaluminite and Alunite: A Possible Cause of Sulfate Retention by Acid Soils, Soil Science Society of American Proceedings 1977;41:686-92.
- [41] Nordstrom DK. The Effect of Sulfate on Aluminum Concentrations in Natural Waters: Some Stability Relations in the System $\text{Al}_2\text{O}_3\text{-SO}_3\text{-H}_2\text{O}$ at 298 K, Geochimica et Cosmochimica Acta 1982;46:681-92.

IntechOpen

